ACS APPLIED NANO MATERIALS

www.acsanm.org Article

Quantum Transport in DNA Heterostructures: Implications for Nanoelectronics

Sunil R. Patil,* Hashem Mohammad, Vivek Chawda, Niraj Sinha, Reman Kumar Singh, Jianqing Qi, and M P. Anantram

Cite This: *ACS Appl. Nano Mater.* 2021, 4, 10029–10037 Read Online

ACCESS | Metrics & More | Article Recommendations | Supporting Information

ABSTRACT: Understanding quantum transport through DNA-based heterostructures is a key to advancing the field of DNA nanoelectronics, where quantum interference would play a significant role. Electronic "barriers" and "wells" can be constructed in DNA using adenine–thymine (AT) and guanine–cytosine (GC) base pairs, respectively, as their ionization potentials differ significantly. We investigate the influence of the width of barriers and wells on hole transport. Density functional theory calculations are performed on energy-minimized DNA structures, followed by quantum transport calculations including decoherence. The device physics is probed by constructing a model Hamiltonian and selectively turning off long-range and interstrand interactions. Major outcomes of the study include the following: (1) DNA heterostructures complement the solid-state semiconductor counterparts; that is, conductance decreases sharply and marginally with an increase in barrier and well width, respectively; (2) quantum interference in DNA heterostructures is robust, as seen by clear peaks in the transmission resonance even with decoherence; (3) DNA conformation has a profound role in deciding the conductance of equivalent heterostructures; and (4) structural differences lead to closer HOMO energy levels and more delocalized states. As a result, transport can be efficient in some strands even with weaker $\pi-\pi$ orbital overlap.

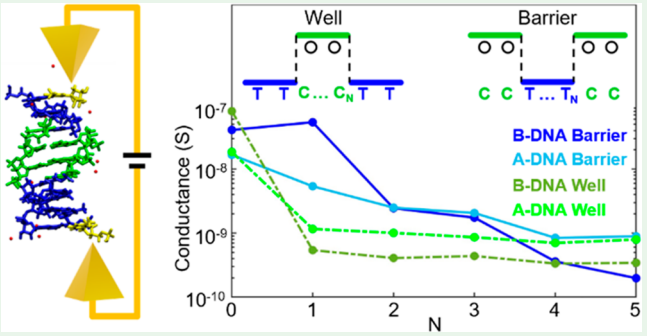

KEYWORDS: *DNA, Nanoelectronics, Heterostructures, Quantum Transport, Multiscale Modeling*

1. INTRODUCTION

The natal function of storing and transmitting information on deoxyribonucleic acid (DNA) by pairing and stacking characteristics of its bases kindles the idea that it can also carry electrical signals. DNA offers precise self-assembly and molecular recognition at the nanoscale, which can drive the fabrication of molecular devices based on quantum interference.[1−3] Therefore, it is appealing to use such features to design devices capable of processing information and signals.[4−6] The emergence of 2D and 3D DNA structures will also instigate ideas for the 3D integration of DNA-based electronics. Apart from this, these devices offer biocompatibility[7] and the possibility of electronics beyond lithography limits.[1] The electronic conductivity of the DNA molecule can be measured with DNA bridging the carbon nanotube gap[8] and single-molecule break junction.[9,10] Additionally, recent experiments and modeling studies show the potential to detect methylation,[11,12] mutations,[13] and mismatches[14] by measuring a single DNA molecule's conductance. Better understanding and prediction of a given DNA molecule's electronic conductivity would further expedite the engineering of DNA-based electronic systems and sensors.

Heterostructures are basic building blocks in electronic devices; therefore, DNA heterostructures are key to DNA-based nanoelectronics. The distinct electronic properties of the different DNA bases lead to the idea of nanostructured *wells*, *barriers*, and *superlattices*.[1−3] The vertical ionization potential (IP) values (in eV) in the gas phase for the four bases and base pairs when isolated are G (7.91) < A (8.30) < C (8.74) < T (9.05) and GC (7.28) < AT (7.86), respectively.[15,16] Since the AT (GC) base pair has a higher (lower) ionization potential than GC (AT), it can be treated as a "barrier" ("well") for hole transport.[2,3] Therefore, one can think of quantum wells and barriers constructed by engineering the DNA sequence. We can expect DNA-based heterostructures exhibiting transmission resonances akin to double barrier resonant tunneling diodes and superlattices built from conventional semiconductor heterostructures. Adessi et al.[3] and Qi et al.[2]

Received: April 21, 2021
Published: September 24, 2021

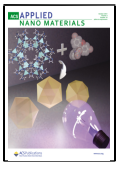

https://doi.org/10.1021/acsanm.1c01087
ACS Appl. Nano Mater. 2021, 4, 10029–10037

reported resonant tunneling and found a length-independent maximum transmission in the purely coherent regime. Additionally, coherent effects play a key role in charge transport in DNA.[17] However, decoherence may wash out these quantum interference effects. Therefore, quantum interference phenomena in electronic barriers and wells where decoherence plays a role need to be investigated.

Concerning charge transport through DNA (hence through DNA-based heterostructures), most investigators seem to agree that the interbase $\pi-\pi$ coupling in DNA could provide a pathway for charge transport along the bases.[1−3,18−20] Accordingly, B-DNA is expected to conduct better among all the DNA conformations. However, recent studies have challenged this understanding,[9,10] where higher conductance is observed in conformations other than B-DNA, despite having relatively weaker interbase $\pi-\pi$ coupling.[18] These studies indicate distinct and/or additional charge transport pathways in conformations other than B-DNA. Additionally, the backbone and its environment can influence DNAs' electronic behavior, such as solvent and counterions.[21−24] Therefore, it would be interesting to probe the charge transport mechanism in DNA heterostructures considering the effect of conformation, backbone, and solvent.

Against this backdrop, we present a critical study of quantum transport (where interference is significant) in electronic barriers and wells formed by sequence engineering in DNA. Mainly, we investigate the influence of the width of the barrier and well. We employ a combination of density functional theory (DFT) and Green's function-based quantum transport calculations including decoherence. Apart from the most common B-conformation, we also study quantum transport in the A-conformation of DNA heterostructures, as dry (relatively dehydrated) DNA exhibits A-conformation.[25] We analyze the role of long-range and interstrand interactions by constructing a model Hamiltonian. The paper is organized as follows. We first present an overview of the methodology employed to obtain the electronic Hamiltonian, model Hamiltonian, and conductance. Next, we present and discuss the conductance variation for barriers and wells. We conclude the paper by discussing the significance of the results and the main findings of our work.

2. METHODS

The sequences 3′-CCCT$_N$CCC-5′ (CT$_N$C) and 3′-TTTC$_N$TTT-5′ (TC$_N$T) are considered as barrier and well sequences for hole transport, where N defines the width of the barrier and well regions, respectively. We obtained the atomic coordinates of DNAs from Nucleic Acid Builder (NAB) in AMBER 16[26] with one extra base pair (GC for CT$_N$C and AT for TC$_N$T sequences) at each end to avoid the edge effects. We used 100% water and 85% ethanol + 15% water as explicit solvents for B- and A-DNA, respectively. For solvent with an ethanol + water mixture, PACKMOL[27] was used to obtain initial frames with packed molecules in a 60 Å × 60 Å × 60 Å cubic solvation box. General Amber Force Field (GAFF)[28] was used to account for interactions involving ethanol. For water as a solvent, the B-DNA structure was solvated with a truncated octahedron box of the SPC/E water model, the size of which was determined from the minimum buffer distance of 11 Å. We introduced sodium (Na) counterions to neutralize the negatively charged phosphate groups. Additionally, Na and chlorine (Cl) ions were added randomly to represent a homogeneous mixture with a concentration of 150 mM.[29,30] Joung and Cheatham ion parameters were used for ions.[31] For DNA, the Amber force field with the parmbsc1 correction[32] was used. The system was then energy-minimized in two steps with a 9 Å cutoff for nonbonding interactions. In stage 1, DNA was restrained with a force of 25 kcal/mol·Å^2 for the first 1000 cycles. In stage 2, the entire system was minimized for a further 1000 cycles. Each stage of energy minimization involves 500 steps of the steepest descent method followed by 500 steps of the conjugate gradient method. Next, we imported the molecule with solvent and counterions into GaussView5.[33] We deleted the extra base pairs at the two ends, excess salt ions (the closest ions required to neutralize the DNA molecule were kept), and solvent molecules. We used DFT calculations with the B3LYP functional[34] and the 6-31G(d,p) basis set within GAUSSIAN09[35] to obtain the Fock (F) and overlap (S) matrices for the given DNA molecule. We modeled the solvent effect within the polarizable continuum model.[36] The dielectric constant of the ethanol−water mixture (ϵ_m) is determined by considering only the linear dependence on mole fractions in the Jouyban-Acree model,[37] i.e., $\epsilon_m = \phi\epsilon_w + (1-\phi)\epsilon_{eth}$. In this equation, ϕ is the mole fraction of water in the mixture, ϵ_w is the dielectric constant of water, and ϵ_{eth} is the dielectric constant of ethanol. For the 85% ethanol + 15% water mixture, we used an effective dielectric constant of 32.877. The F and S matrices extracted from DFT calculations are transformed to the orthogonal basis using Löwdin transformation:[24,38]

$$H = S^{-1/2} F S^{-1/2} \tag{1}$$

Here, the diagonal elements of H represent the energy levels at each atomic orbital, and the off-diagonal elements correspond to the coupling between the different atomic orbitals. Mathematically, it can also be expressed as

$$H = H^{D}_{DNA} + H^{D}_{CI} + H^{OD}_{DNA} + H^{OD}_{CI} + H^{OD}_{CI\text{-}DNA} \tag{2}$$

where the diagonal matrices H^{D}_{DNA} and H^{D}_{CI} correspond to all the atoms in DNA (base + backbone) and counterions, respectively. The off-diagonal matrix H^{OD}_{DNA} represents interactions between the basis states of each atom with the basis states of the rest of the DNA atoms. Similarly, H^{OD}_{CI} is the off-diagonal matrix representing interactions among the counterions and $H^{OD}_{CI\text{-}DNA}$ represents the interaction between counterions and DNA. The matrices H^{D}_{DNA}, H^{D}_{CI}, H^{OD}_{CI}, H^{OD}_{DNA}, and $H^{OD}_{CI\text{-}DNA}$ are defined as

$$H^{D}_{DNA} = \sum_{k=1\to b_n, n=1\to N_{DNA}} \epsilon_{k,n} C^{\dagger}_{k,n} C_{k,n}$$

$$H^{D}_{CI} = \sum_{k=1\to b_n, m=1\to N_{CI}} \epsilon_{k,m} C^{\dagger}_{k,m} C_{k,m}$$

$$H^{OD}_{DNA} = \sum_{n,n'=1\to N_{DNA}, i,j=1\to b_n} t_{i,n:j,n'} (C^{\dagger}_{i,n} C_{j,n'} + \text{c. c.})$$

$$H^{OD}_{CI} = \sum_{n=1\to N_{CI}, m'=1\to N_{CI}, i,j=1\to b_n} t_{i,n:j,m'} (C^{\dagger}_{i,n} C_{j,m'} + \text{c. c.})$$

and

$$H^{OD}_{CI\text{-}DNA} = \sum_{n=1\to N_{DNA}, m'=1\to N_{CI}, i,j=1\to b_n} t_{i,n:j,m'} (C^{\dagger}_{i,n} C_{j,m'} + \text{c. c.}) \tag{3}$$

Here, the total number of atoms in the system is given as $N_A = N_{DNA} + N_{CI}$, where N_{DNA} and N_{CI} are the number of atoms in the DNA and counterions, respectively. $B = \sum_{n=1}^{N_A} b_n$ is the total number of basis functions used to represent the entire system for DFT calculations, where b_n is the number of basis states of the nth atom. $\epsilon_{k,n}$ is the kth on-site energy of the nth atom. The interaction between the ith basis state of the nth atom and the jth basis state of the m'th atom is denoted by $t_{i,n:j,m}$, and c.c. stands for the Hermitian conjugate. $C^{\dagger}$ and C are the creation and annihilation operators, respectively.

The transmission, T_{eff}, and density of states (DOS) are then determined using the Green's function approach within the Büttiker framework.[24] The retarded Green's function (G^r) was found by solving the following equation:

$$[E - (H + \Sigma_L + \Sigma_R + \Sigma_B)] G^r = I \tag{4}$$

https://doi.org/10.1021/acsanm.1c01087
ACS Appl. Nano Mater. 2021, 4, 10029−10037

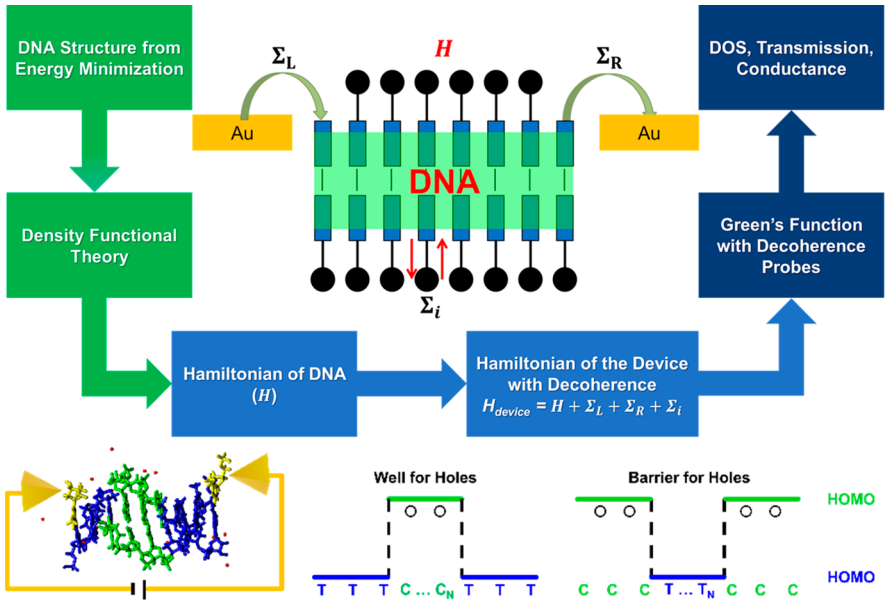

Figure 1. Modeling approach and the problem under investigation.

where E is the energy level and and $\Sigma_{L(R)}$ is the left (right) contact self-energy, representing the coupling strength of the DNA to the left (right) contact by which charge enters and leaves the DNA. The self-energy of the phase-breaking decoherence probe is defined as Σ_B. In this study, we employ a new atomic partitioning scheme that treats each atom in the system as a block.

Molecular dynamics simulations have shown that the energy levels of the DNA fluctuate. The time-averaged behavior of these fluctuations leads to energy broadening,[39] which is qualitatively obtained by the decoherence probes that we employ in our study. The decoherence probes are artificial probes connected to the DNA. Electrons flow from the DNA into these probes which are maintained at thermal equilibrium, as given by Fermi statistics. These electrons are reinjected from the probe back into the DNA such that the total current in the decoherence probe is zero. This process effectively causes the electron's phase to decohere. We consider a uniform decoherence rate of Σ_B = 10 meV at each site/block. We choose this value because it is consistent with estimates for decoherence from Parsons' quantum molecular dynamics simulations[40] and reference.[24] The contact-DNA self-energy, $\Sigma_{L(R)}$ = 100 meV, is added to the ends of the DNA, i.e., at 5′ (3′) end at the backbone-base atoms to inject and extract electrons from the left (right) contact. The contact sites are shown in Figure S1 in the Supporting Information.

We assume that the difference between the left and right electrodes' chemical potential is relatively small, and so the linear response transport is assumed. The conductance is thus defined as

$$G(E_F) = G_o \int_{-\infty}^{+\infty} T_{eff}(E) \frac{-\partial f(E - E_F)}{\partial E} dE \quad (5)$$

where G_o is the quantum of conductance, i.e., $2e^2/h$ (e is the charge on an electron and h is Planck's constant) and f is the Fermi distribution function. Our computational models and approach are summarized in Figure 1, and further details can be found in ref 41.

3. RESULTS AND DISCUSSION

The location of E_F with respect to the energy levels of the DNA molecule is determined by factors such as the IP values of DNA bases and the work function of metal electrodes[42] and the configuration of DNA with respect to the electrodes. The configuration accounts for the number of DNA atoms in contact and their relative orientation with respect to the electrode. These factors determine the partial charge transfer between DNA and electrodes,[43] which determines E_F. By comparing the IP values of DNA bases and accounting for gold electrodes with a work function of 5.3 eV, we expect the E_F location to be in the HOMO−LUMO gap, closer to the HOMO of the DNA. As emphasized in previous work,[43] partial charge transfer between the electrode and DNA brings E_F closer to the HOMO. In this study, we assumed that the E_F shifts similarly for all strands with respect to their respective HOMO energy. This scenario can occur if we have a three-terminal setup (see Figure 2): it consists of left and right

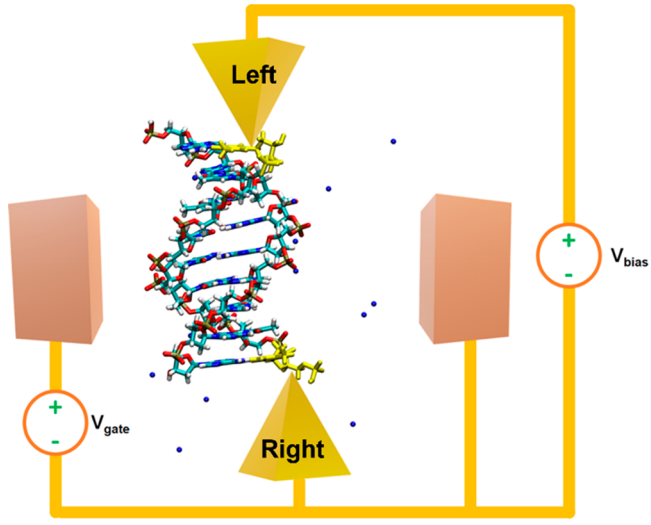

Figure 2. Three-terminal setup having a gate electrode that can sweep the Fermi energy from HOMO to LUMO.

electrodes across which conductance is calculated and the gate electrode that can sweep the E_F from HOMO to LUMO energies. In presenting our results in Figure 3a−e, we assumed that the E_F is gated such that it is at the HOMO of each strand and a small bias is applied across the left and right electrode. The trend in conductance obtained for E_F = HOMO (Figure 3e) also holds when E_F = HOMO + 100 meV (Figure S2 in the Supporting Information).

https://doi.org/10.1021/acsanm.1c01087
ACS Appl. Nano Mater. 2021, 4, 10029−10037

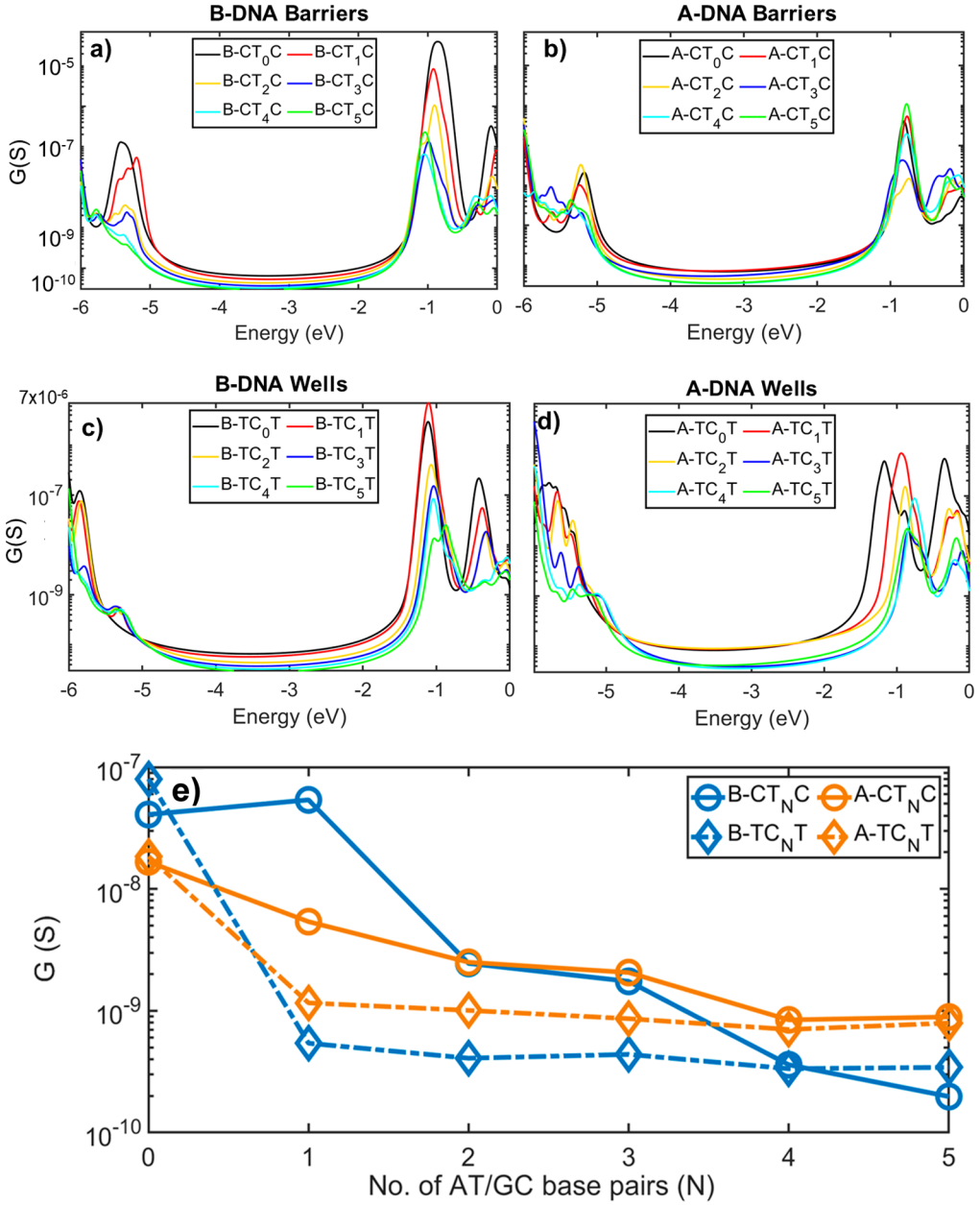

Figure 3. Conductance variation with Fermi energy for (a) B-DNA barriers, (b) A-DNA barriers, (c) B-DNA wells, and (d) A-DNA wells. (e) Conductance at HOMO of B-DNA (blue) and A-DNA (orange) barriers (solid) and wells (dashed) as a function of barrier/well width *N*. Shorter B-DNAs conduct better than A-DNA, whereas longer A-DNAs conduct better than B-DNAs.

Figure 3a–d shows conductance variation with E_F, and Figure 3e shows conductance variation at respective HOMO energies for DNA as a function of the width of the barrier and well regions (N = 0–5). See Table S1 of Supporting Information for HOMO energy levels. These DNA molecules exhibit conductance within the range of 0.2 to 80 nS, which lies within the broad range of reported experimental values of 10^{-13} and 10^{-5} S.[19,42,44−46] A prior modeling study[2] on a DNA strand without a backbone also showed that the conductance decreases monotonically with increasing N for barriers. However, the work did not consider the effect of DNA conformation, backbone, solvent, and counterions. Reference 24 considered the backbone but failed to include the impact of the solvent around the DNA. We also note that the experiments with increasing AT base pairs found that the conductance decreases with an increase in N.[10,42,45] In general, we also find that DNA conductance decreases with increasing N. However, there are important exceptions, differing from prior studies. We find that for B-CT$_N$C, the conductance surprisingly increases from 41 to 54 nS as N changes from N = 0 to N = 1 (Figure 3e). That is, the inclusion of a single AT barrier increases conductance. Also, note that the longer A-DNA heterostructures conduct better than B-DNAs. The crossover point occurs upon introducing a GC base pair for well sequences, as against two AT base pairs for barrier sequences. We confirmed that these observations are consistent even in the vicinity of HOMO level to account for variation in the Fermi energy in experiments (see Figure S2 in the Supporting Information) and for textbook DNAs (see Figure S3 in the Supporting Information). Next, we explain these observations one by one.

https://doi.org/10.1021/acsanm.1c01087
ACS Appl. Nano Mater. 2021, 4, 10029−10037

First, we look at the HOMO−LUMO energy levels and the DOS along the DNA length for the well sequences (Figure 4). For brevity, we are restricting our discussion to N = 0, 1, 3, and 5 cases. In general, the HOMO−LUMO gap for B-DNA (A-DNA) decreases with the increasing number of GC base pairs, from 5.80 eV (5.45 eV) for N = 0 to 5.19 eV (5.11 eV) for N = 5; see Figure 4a. When we introduce the GC base pairs, additional energy levels are introduced in the HOMO band (−5.1 to −5.5 eV), as the HOMO in DNA mainly lies on guanines.[18,47−49] In Figure 4b−i, we plot the DOS as a function of energy along the DNA length. Although the HOMO orbitals primarily reside on GC base pairs, that is, in the middle of these molecules, a smaller orbital component is on the nearby AT base pairs. This localization is true for both conformations, which we can see for N = 1, 3, and 5. However, in A-DNAs (Figure 4c−e), the HOMO orbital localization on AT base pairs is considerably higher (Figure 4g−i). The HOMO wave functions plotted in Figure S4 in the Supporting Information further support this observation. We also explore the HOMO band of well sequences by plotting the decoherent transmission T_{eff} variation in the HOMO band in Figure 5. The HOMO band of well structures shows that the number of transmission peaks is consistent with the number of GC base pairs between the AT barriers. As the well width increases, the overall structure length increases, increasing scattering and lowering the transmission (conductance) by small amounts. The small amount of variation indicates that the quantum interference phenomena of resonant tunneling remain effective. Another interesting observation is that B-DNA displays a relatively uniform distribution of transmission peaks, whereas A-DNA looks disordered (Figure 5). The transmission peaks are better resolved in coherent transmission plots, as presented in Figure S5 in the Supporting Information. While it is tempting to think that the transmission spectrum for A-DNA is due to decoherence, we believe that the primary reason is its structure, which makes the energy levels nonuniform when compared to the B-DNA case. We can also see from Figure 4a that the HOMO levels are energetically more closely spaced for A-DNA than for B-DNA. For N = 5 (3), $E_{HOMO} - E_{HOMO-2}$ is 59 meV (75 meV) for A-DNA but 96 meV (120 meV) for B-DNA. These observations and relatively more delocalized HOMO orbitals support our finding that A-DNA heterostructures conduct better than B-DNA.

Next, we explain the barrier case. Increasing the number of AT base pairs decreases the conductance (Figure 3e) as AT base pairs function as a barrier for holes. However, for the B-DNA, an exception arises at N = 1, which we will address shortly. Figure 6a shows that the HOMO−LUMO gap decreases as N changes from 0 to 5. In contrast to the well case, Figure 6a shows that when we introduce the AT base pairs, a corresponding number of energy levels are introduced deeper in the HOMO band (between −5.7 and −5.9 eV; also see Figure 6b−i). This observation is also reflected in coherent transmission plots for barriers in Figure S6 in the Supporting Information. As the HOMO mainly lies on guanines, the HOMO level is relatively unchanged. For N = 3, the HOMO band of A-DNA (Figure 6d) is more delocalized than that of B-DNA (Figure 6h). For N = 5, we see that the HOMOs are mainly localized on the GC base pairs (Figure 6e,i). HOMO distributions presented in Figure S7 in the Supporting Information also support this. Furthermore, like the well case, we find that HOMO levels are energetically more closely

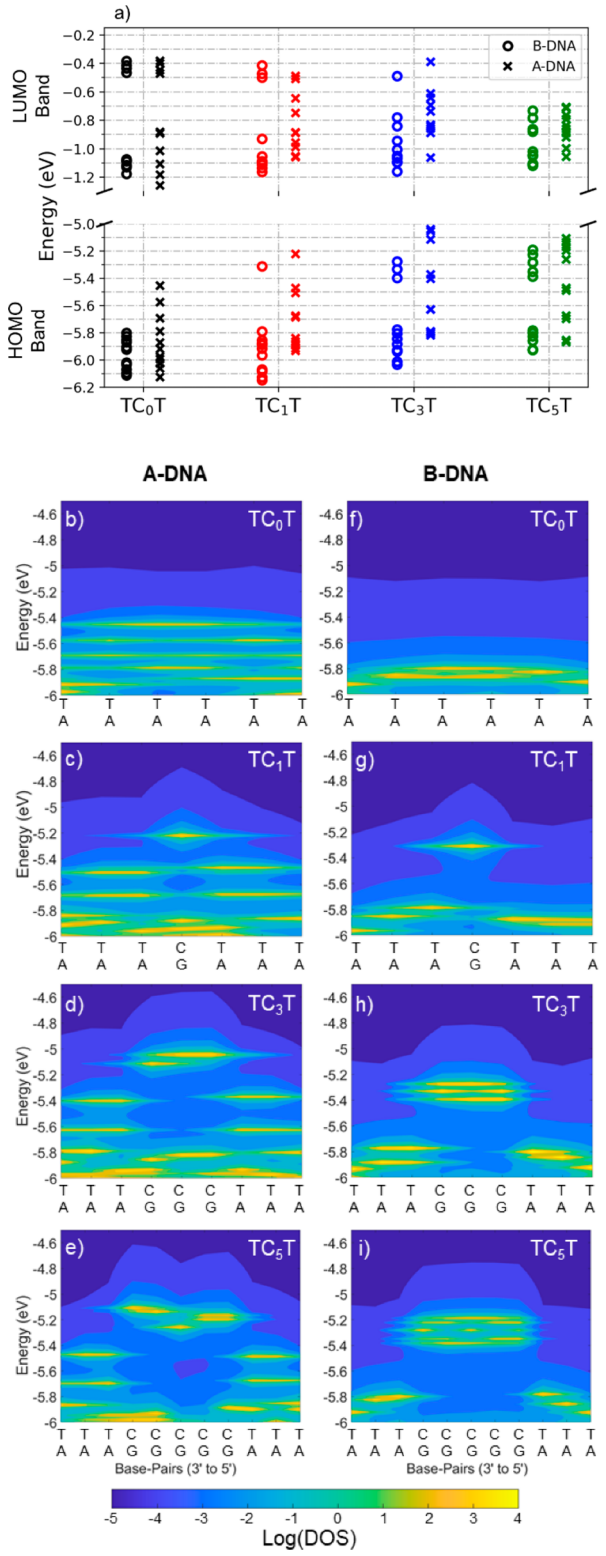

Figure 4. (a) HOMO−9: HOMO and LUMO: LUMO+9 energy levels for A- and B-DNA for well sequences. DOS along the length of (b−e) A-DNA and (f−i) B-DNA. B-DNA HOMO orbitals are localized mainly on central GC base pairs, whereas A-DNA HOMO orbitals are relatively more delocalized (extended to nearby AT base pairs). The left and right ends of the sequences are 3′ and 5′ ends, respectively.

https://doi.org/10.1021/acsanm.1c01087
ACS Appl. Nano Mater. 2021, 4, 10029−10037

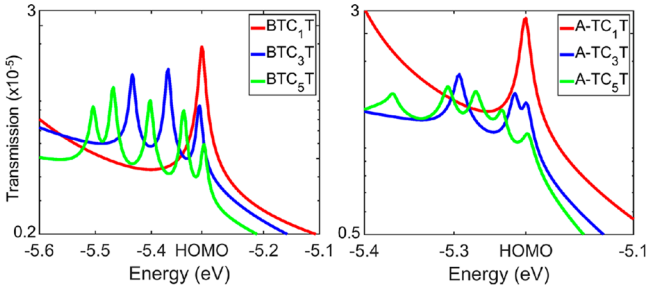

Figure 5. Decoherent transmission in HOMO band regions for different well widths. (Left) A-DNA and (right) B-DNA. HOMOs are aligned to the $N = 1$ case.

spaced in A-DNA than in B-DNA. For $N = 5$ (3), $E_{HOMO} - E_{HOMO-2}$ is 62 meV (33 meV) for A-DNA and is 152 meV (95 meV) for B-DNA.

The B-DNA barrier with $N = 1$ conducts better than $N = 0$; that is, a longer DNA with a barrier conducts better than shorter DNA without a barrier. Upon introducing a single AT base pair, the HOMO and HOMO−1 energy levels almost become degenerate around −5.2 eV (Figure 6a), and the gap between them has decreased from 60 to 18 meV. One of the significant effects of decoherence is to broaden energy levels. Hence, applying the 10 meV decoherence helps overcome the 18 meV separation between the two levels.[24] In other words, the presence of decoherence makes these energy levels accessible for holes to traverse. Figure S6a in the Supporting Information shows that the coherent transmission at HOMO for $N = 1$ is smaller than that of the $N = 0$ case. The DOS plots along the DNA length are shown in Figure 6f,g, respectively for $N = 0$ and 1. The DOS is more uniformly distributed in the case of $N = 1$ of B-DNA. Also, at the injection site, DOS is higher for $N = 1$ than for $N = 0$. For A-DNA, the relatively smaller DOS with nonuniform distribution for $N = 1$ supports the expected smaller conductance than the $N = 0$ case. The DOS in the HOMO band, as shown in Figure 6b,c, also substantiates this. The line plot in Figure S8 in the Supporting Information further validates this.

To rule out that the higher conductance exhibited by longer A-DNA heterostructures is due to long-range interactions, we formulated a model Hamiltonian H' that excludes long-range interactions.

$$H' = H^{D}_{DNA} + H^{D}_{CI} + H^{OD'}_{DNA} + H^{OD}_{CI} + H^{OD}_{CI\text{-}DNA} \quad (6)$$

where

$$H^{OD'}_{DNA} = \sum_{q=1\to N_b, q'=1\to 6, i,j=1\to b_n} t_{i,q:j,q'}(C^{\dagger}_{i,q}C_{j,q'} + c.\,c.)$$

Here, N_b is the total number of bases in the DNA molecule (22 for N = 5); $q' = [q_U q_L q_A q_{AU} q_{AL} q_{BB}]$ represents an array of bases and part of the backbone allowed to interact with a given base q. q_U and q_L are upper and lower bases, respectively, in the same strand as base q. q_A is the adjacent base in the complementary strand; q_{AU} and q_{AL} are upper and lower bases to q_A, respectively, and q_{BB} corresponds to the part of the DNA backbone which is covalently bonded to the base q. These constituents of DNA are depicted in Figure 7 (left). Note that we set all other interactions to zero in the model Hamiltonian. We further extend this analysis to understand the role of interactions of interstrand bases. The model Hamiltonian approach enables us to switch on and off particular interactions

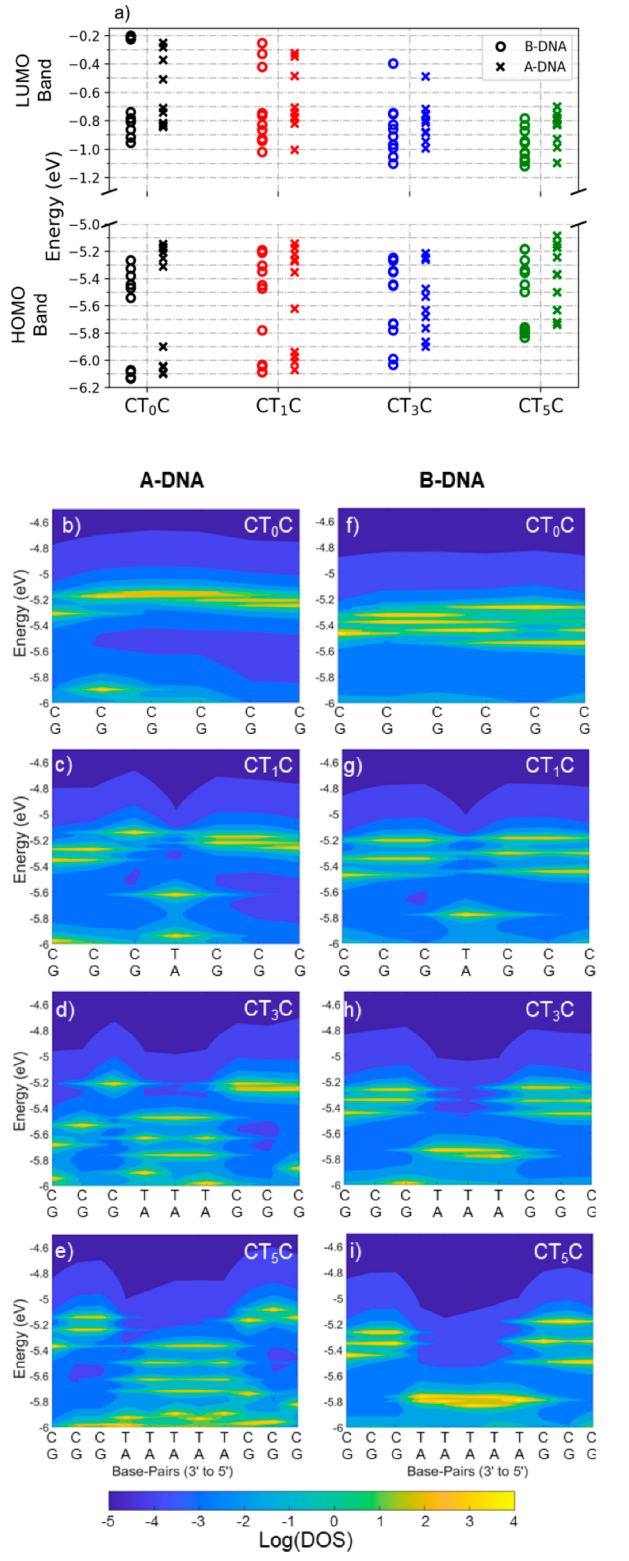

Figure 6. (a) HOMO−9: HOMO and LUMO: LUMO+9 energy levels for A- and B-DNA barrier sequences. DOS along the length for (b−e) A-DNA and (f−i) B-DNA. The A-DNA HOMO band extends further along the length of the molecule as against B-DNA.

selectively and is readily extendible for other systems. We compare the conductance in Figure 7 (right) through the longest molecule representing the barrier and well, that is, the $N = 5$ case for A-DNA with model Hamiltonian, H'. The conductance values do not change significantly upon switching

https://doi.org/10.1021/acsanm.1c01087
ACS Appl. Nano Mater. 2021, 4, 10029−10037

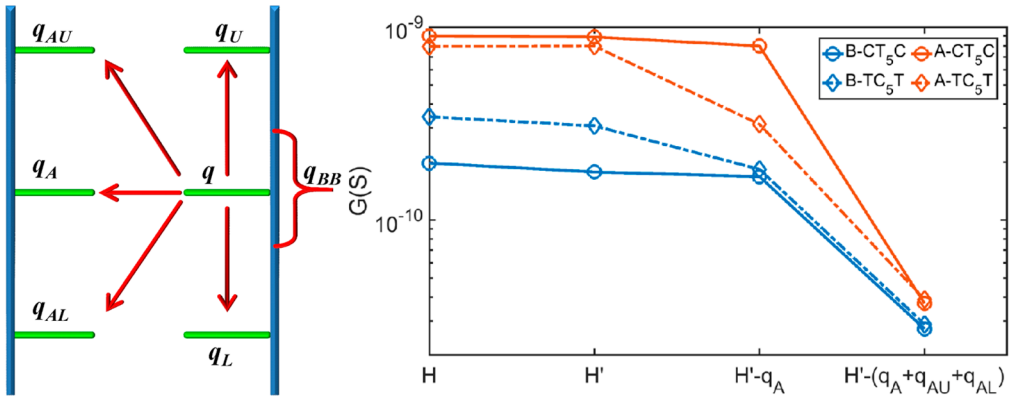

Figure 7. (Left) Constituents of DNA molecule. Blue and green lines represent backbone and bases, respectively. (Right) Conductance is calculated by using H' as defined in eq 6, $H' - q_A$, $H' - (q_A + q_{AU} + q_{AL})$ and is compared with the conductance obtained using H in eq 2. $H' - q_A$ represents H' without $q \leftrightarrow q_A$ interactions. Similarly, $H' - (q_A + q_{AU} + q_{AL})$ represents H' without $q \leftrightarrow q_A$, $q \leftrightarrow q_{AU}$, and $q \leftrightarrow q_{AL}$ interactions.

off the long-range interactions. We have extended this analysis by switching off the interactions between interstrand bases. Switching off the interactions between complementary bases, q_A begins to decrease the conductance. This leads to a relatively larger conductance reduction for the well case compared to that for the barrier case. This could arise in the well case from the combination of two facts: (i) the large DOS in the complementary strand (Figure S10a,b and (ii) the larger hopping parameter on an average with the q_A interaction compared to q_{AU} and q_{AL}, as can be seen from Figure S10c in the Supporting Information. Finally, switching off all the interstrand interactions causes a substantial decrease in conductance for barrier and well cases. However, even after removing all the interstrand interactions, the A-DNA heterostructure exhibits higher conductance for both the barrier and the well sequences. This result implies that long-range interactions do not contribute to quantum transport, whereas the short-range interstrand interactions play a significant role.

Present understanding of charge transport through DNA has been that it is mainly led by the $\pi-\pi$ interactions of stacked bases, which decays with increasing length[18,50] and the AT content.[24,42] Therefore, B-DNA is believed to conduct better due to better base pair alignment and hence the better $\pi-\pi$ couplings compared to A-DNA.[18] Surprisingly, we find that some longer A-DNA heterostructures conduct better than B-DNAs with the same sequence. This finding also implies that the decrease in conductance with length is distinct in B- and A-DNA heterostructures. We find that the conductance of B-DNA barriers decreases more sharply compared to that of A-DNA. Moreover, the decrease in conductance in both the conformations upon switching off interstrand interactions indicates that the interactions between complementary strands of stacked bases do play a role even in A-DNA. However, we find the closely distributed energy levels and the higher spatial delocalization of HOMO in A-DNA heterostructures to be the main factors responsible for its higher conductance. Structurally, the A- and B-DNA mainly differ in slide, tilt, and helical rise per base pair.[51,52] As the length of the molecule along the A-DNA's helical axis increases by 2.6 Å compared to 3.4 Å for B-DNA, their helical length difference is $N \times 0.8$ Å. Therefore, we hypothesize that the smaller helical rise and twist and the larger diameter in A-DNA heterostructures compared to those of B-DNA may create energetically closer HOMO levels distributed over the DNA length, leading to a higher conductance. This hypothesis could also explain previously reported higher conductance in non-B-DNA conformations.[9,10]

4. CONCLUSIONS

In this work, we study quantum transport through DNA-based quantum wells and barriers using a combination of atomistic simulations and Green's function-based charge transport calculations including decoherence. We formed the DNA-based quantum well and barrier with sequences 3′-TTTC$_N$TTT-5′ and 3′-CCCT$_N$CCC-5′, respectively, where N varies from 0 to 5. Overall, we find that the strands' resistance is large and varies by over 2 orders of magnitude. We showed that these heterostructures complement their semiconductor-based counterparts. Increasing the well width (N) shows a small decrease in conductance. On the other hand, the decrease in conductance with the increase in barrier width is substantial. Our model, which includes decoherence, shows that these heterostructures exhibit robust quantum interference, as seen by clear peaks in the transmission resonance. It also shows that the conductance depends significantly on barrier width. The role of DNA conformation is also investigated. We find that B-DNA's conductance decreases more sharply with barrier width than does that of A-DNA, which experiments should be able to verify. In deviation from conventional expectation, the smallest barrier ($N = 1$) shows a conductance higher than that of the no barrier case in B-DNA. B-DNA quantum wells have large electronic coupling between consecutive GC base pairs (hybridization). As a result, B-DNA quantum wells have a uniform distribution of conductance peaks, whereas they are disordered for A-DNA. Model Hamiltonian analysis suggests that the interstrand interactions play a major role in quantum transport in DNA, and long-range interactions are insignificant. However, in A-DNA, we find that the HOMO levels are energetically more closely spaced, and the HOMO orbitals are spatially more delocalized. Therefore, we conclude that the energetically closer HOMO levels and the larger spatial delocalization of density of states in the conduction energy window may lead to higher conductance in A-DNA heterostructures. These two properties of A-DNA can overcome its relatively weaker $\pi-\pi$ coupling between orbitals on neighboring bases. This observation presents a new understanding of charge transport particularly in DNAs in addition to the idea of charge transport dominated by the $\pi-\pi$ interactions of stacked bases. We attribute these

https://doi.org/10.1021/acsanm.1c01087
ACS Appl. Nano Mater. 2021, 4, 10029−10037

properties to the structural differences between DNA conformation in otherwise identical strands. The analysis and computational results demonstrate that DNA-based heterostructures complement the solid-state semiconductor counterparts and exhibit robust quantum interference, where the DNA conformation can play a significant role.

■ ASSOCIATED CONTENT

Supporting Information

The Supporting Information is available free of charge at https://pubs.acs.org/doi/10.1021/acsanm.1c01087.

Contact locations for charge transport calculations; conductance variation at E_{HOMO} + 100 meV; conductance variation for textbook DNAs; HOMO energies of the molecules; HOMO distributions for well sequences; coherent transmission for well sequences; coherent transmission for barrier sequences; HOMO distribution for barrier sequences; comparative DOS analysis for smallest B-DNA barrier (N = 1) and no barrier case (N = 0); extended model Hamiltonian analysis; strandwise DOS and hopping parameters (PDF)

■ AUTHOR INFORMATION

Corresponding Author

Sunil R. Patil − *Department of Physics, Institute of Science, Nagpur, MS 440008, India;* orcid.org/0000-0002-4112-1867; Email: phy.patil@iscnagpur.ac.in

Authors

Hashem Mohammad − *Department of Electrical and Computer Engineering, University of Washington, Seattle, Washington 98195, United States;* orcid.org/0000-0002-9783-2326

Vivek Chawda − *Department of Mechanical Engineering, Indian Institute of Technology, Kanpur, UP 208 016, India*

Niraj Sinha − *Department of Mechanical Engineering, Indian Institute of Technology, Kanpur, UP 208 016, India;* orcid.org/0000-0001-6600-9313

Reman Kumar Singh − *Department of Chemistry, Indian Institute of Technology, Bombay, MS 400076, India*

Jianqing Qi − *Department of Electrical and Computer Engineering, University of Washington, Seattle, Washington 98195, United States*

M P. Anantram − *Department of Electrical and Computer Engineering, University of Washington, Seattle, Washington 98195, United States*

Complete contact information is available at: https://pubs.acs.org/10.1021/acsanm.1c01087

Notes

The authors declare no competing financial interest.

■ ACKNOWLEDGMENTS

S.P. acknowledges the support from SERB, India Grant No. TAR/2018/001188, and H.M. acknowledges a Kuwait University Fellowship. V.C. performed some of these calculations using the HPC facility at IIT Kanpur. M.P.A. acknowledges NSF Grant Nos. 1807391 (SemiSynBio Program) and 2036865 (Future of Manufacturing) for support.

■ REFERENCES

(1) Porath, D.; Lapidot, N.; Gomez-Herrero, J. Charge Transport in DNA-Based Devices. In *Introducing Molecular Electronics*; Cuniberti, G., Richter, K., Fagas, G., Eds.; Springer: Berlin, 2005; p 411.

(2) Qi, J.; Rabbani, M. G.; Edirisinghe, S.; Anantram, M. P. Transport of charge in DNA heterostructures. *11th IEEE International Conference on Nanotechnology*, 2011; pp 487−491.

(3) Adessi, C.; Walch, S.; Anantram, M. P. Environment and structure influence on DNA conduction. *Phys. Rev. B: Condens. Matter Mater. Phys.* **2003**, *67*, 081405.

(4) Niemeyer, C. M. Nanoparticles, proteins, and nucleic acids: biotechnology meets materials science. *Angew. Chem., Int. Ed.* **2001**, *40*, 4128−4158.

(5) Niemeyer, C. M. DNA as a material for nanotechnology Angew. *Angew. Chem., Int. Ed. Engl.* **1997**, *36*, 585−587.

(6) Di Mauro, E.; Hollenberg, C. P. DNA technology in chip construction. *Adv. Mater.* **1993**, *5*, 384−386.

(7) Liedl, T.; Sobey, T. L.; Simmel, F. C. DNA-based nanodevices. *Nano Today* **2007**, *2*, 36−41.

(8) Guo, X.; Gorodetsky, A. A.; Hone, J.; Barton, J. K.; Nuckolls, C. Conductivity of a single DNA duplex bridging a carbon nanotube gap. *Nat. Nanotechnol.* **2008**, *3*, 163−167.

(9) Artés, J. M.; Li, Y.; Qi, J.; Anantram, M. P.; Hihath, J. Conformational gating of DNA conductance. *Nat. Commun.* **2015**, *6*, 8870.

(10) Li, Y.; Artés, J. M.; Hihath, J. Long-Range Charge Transport in Adenine-Stacked RNA:DNA Hybrids. *Small* **2016**, *12*, 432−437.

(11) Qi, J.; Govind, N.; Anantram, M. P. The role of cytosine methylation on charge transport through a DNA strand. *J. Chem. Phys.* **2015**, *143*, No. 094306.

(12) Hihath, J.; Guo, S.; Zhang, P.; Tao, N. Effects of cytosine methylation on DNA charge transport. *J. Phys.: Condens. Matter* **2012**, *24*, 164204.

(13) He, L.; Zhang, J.; He, C.; Zhao, B.; Xie, Z.; Chen, W.; Sonawane, M. R.; Patil, S. R. Electronic characteristics of BRCA1 mutations in DNA. *Biopolymers* **2021**, *112*, e23465.

(14) Wohlgamuth, C. H.; McWilliams, M. A.; Slinker, J. D. Temperature Dependence of Electrochemical DNA Charge Transport: Influence of a Mismatch. *Anal. Chem.* **2013**, *85*, 1462−1467.

(15) Caruso, T.; Carotenuto, M.; Vasca, E.; Peluso, A. Direct Experimental Observation of the Effect of the Base Pairing on the Oxidation Potential of Guanine. *J. Am. Chem. Soc.* **2005**, *127*, 15040−15041.

(16) Caruso, T.; Capobianco, A.; Peluso, A. The Oxidation Potential of Adenosine and Adenosine-Thymidine Base Pair in Chloroform Solution. *J. Am. Chem. Soc.* **2007**, *129*, 15347−15353.

(17) Landi, A.; Capobianco, A.; Peluso, A. Coherent Effects in Charge Transport in Molecular Wires: Toward a Unifying Picture of Long-Range Hole Transfer in DNA. *J. Phys. Chem. Lett.* **2020**, *11*, 7769−7775.

(18) Endres, R. G.; Cox, D. L.; Singh, R. R. P. Colloquium: The quest for high-conductance DNA. *Rev. Mod. Phys.* **2004**, *76*, 195.

(19) Xiang, L.; Palma, J. L.; Bruot, C.; Mujica, V.; Ratner, M. A.; Tao, N. Intermediate tunnelling–hopping regime in DNA charge transport. *Nat. Chem.* **2015**, *7*, 221.

(20) Liu, T.; Barton, J. K. DNA Electrochemistry through the Base Pairs Not the Sugar−Phosphate Backbone. *J. Am. Chem. Soc.* **2005**, *127*, 10160−10161.

(21) Xie, P.; Liu, K.; Gu, F.; Aoki, Y. Counter-ion effects of A- and B-type poly(dG)·Poly(dC) and poly(dA)·Poly(dT) DNA by elongation method. *Int. J. Quantum Chem.* **2012**, *112*, 230−239.

(22) Kratochvilová, I. DNA and RNA Electronic Properties for Molecular Modifications and Environmental State Diagnostics. In *RNA and DNA Diagnostics*; Springer, 2015; pp 225−239.

(23) Zhuravel, R.; Huang, H.; Polycarpou, G.; Polydorides, S.; Motamarri, P.; Katrivas, L.; Rotem, D.; Sperling, J.; Zotti, L. A.; Kotlyar, A. B.; Cuevas, J. C.; Gavini, V.; Skourtis, S. S.; Porath, D. Backbone charge transport in double-stranded DNA. *Nat. Nanotechnol.* **2020**, *15*, 836−840.

(24) Qi, J.; Edirisinghe, N.; Rabbani, M. G.; Anantram, M. P. Unified model for conductance through DNA with the Landauer-Büttiker formalism. *Phys. Rev. B: Condens. Matter Mater. Phys.* **2013**, *87*, 085404.
(25) Xiao-Hong, L.; Yu-Yu, Z.; Tao, L.; Ke-Lin, W. Further Discussion on Polaron Existence in Dry DNA Chinese. *Chin. Phys. Lett.* **2009**, *26*, 128701.
(26) Case, D. A.; Betz, R. M.; Cerutti, D. S.; Cheatham, T. E., III; Darden, T. A.; Duke, R. E.; Giese, T. J.; Goetz, A. W.; Homeyer, N.; Izadi, S.; Janowski, P.; Kaus, J.; Kovalenko, A.; Lee, T. S.; LeGrand, S.; Li, P.; Lin, C.; Luchko, T.; Luo, R.; Madej, B.; Mermelstein, D.; Merz, K. M.; Monard, G.; Nguyen, H.; Nguyen, H. T.; Omelyan, I.; Onufriev, A.; Roe, D. R.; Roitberg, A.; Sagui, C.; Simmerling, C. L.; Botello-Smith, W. M.; Walker, R. C.; Wang, J.; Wolf, R. M.; Wu, X. *AMBER* 2016.
(27) Martinez, L.; Andrade, R.; Birgin, E. G.; Martinez, J. M. PACKMOL: a package for building initial configurations for molecular dynamics simulations. *J. Comput. Chem.* **2009**, *30*, 2157–2164.
(28) Wang, J.; Wolf, R. M.; Caldwell, J. W.; Kollman, P. A.; Case, D. A. Development and testing of a general amber force field. *J. Comput. Chem.* **2004**, *25*, 1157–1174.
(29) Owczarzy, R.; You, Y.; Moreira, B. G.; Manthey, J. A.; Huang, L.; Behlke, M. A.; Walder, J. A. Effects of sodium ions on DNA duplex oligomers: improved predictions of melting temperatures. *Biochemistry* **2004**, *43*, 3537–3554.
(30) Galindo-Murillo, R.; Roe, D. R.; Cheatham, T. E. Convergence and reproducibility in molecular dynamics simulations of the DNA duplex d(GCACGAACGAACGAACGC) Biochim. *Biochim. Biophys. Acta, Gen. Subj.* **2015**, *1850*, 1041–1058.
(31) Joung, I. S.; Cheatham, T. E., III Determination of alkali and halide monovalent ion parameters for use in explicitly solvated biomolecular simulations. *J. Phys. Chem. B* **2008**, *112*, 9020–9041.
(32) Ivani, I.; Dans, P. D.; Noy, A.; Pérez, A.; Faustino, I.; Hospital, A.; Walther, J.; Andrio, P.; Goñi, R.; Balaceanu, A.; Portella, G.; Battistini, F.; Gelpí, J. L.; González, C.; Vendruscolo, M.; Laughton, C. A.; Harris, S. A.; Case, D. A.; Orozco, M. Parmbsc1: a refined force field for DNA simulations. *Nat. Methods* **2016**, *13*, 55.
(33) Dennington, R.; Keith, T.; Millam, J. *GaussView* 2009.
(34) Becke, A. D. Density-functional thermochemistry. III. The role of exact exchange. *J. Chem. Phys.* **1993**, *98*, 5648–5652.
(35) Frisch, M. J.; Trucks, G. W.; Schlegel, H. B.; Scuseria, G. E.; Robb, M. A.; Cheeseman, J. R.; Scalmani, G.; Barone, V.; Mennucci, B.; Petersson, G. A.; et al. *Gaussian 09*; Gaussian. Inc.: Wallingford, CT, 2009.
(36) Tomasi, J.; Mennucci, B.; Cammi, R. Quantum Mechanical Continuum Solvation Models. *Chem. Rev.* **2005**, *105*, 2999–3094.
(37) Abolghassemi-Fakhree, M. A.; Delgado, D. R.; Martínez, F.; Jouyban, A. The Importance of Dielectric Constant for Drug Solubility Prediction in Binary Solvent Mixtures: Electrolytes and Zwitterions in Water + Ethanol. *AAPS PharmSciTech* **2010**, *11*, 1726–1729.
(38) Mehrez, H.; Anantram, M. P. Interbase electronic coupling for transport through DNA. *Phys. Rev. B: Condens. Matter Mater. Phys.* **2005**, *71*, 115405.
(39) Wolter, M.; Elstner, M.; Kleinekathöfer, U.; Kubař, T. Microsecond Simulation of Electron Transfer in DNA: Bottom-Up Parametrization of an Efficient Electron Transfer Model Based on Atomistic Details. *J. Phys. Chem. B* **2017**, *121*, 529–549.
(40) Parson, W. W. Effects of Free Energy and Solvent on Rates of Intramolecular Electron Transfer in Organic Radical Anions. *J. Phys. Chem. A* **2017**, *121*, 7297–7306.
(41) Qi, J. Modeling Electrical Transport through Nucleic Acids. Ph.D. Dissertation, University of Washington, Seattle, WA, 2015.
(42) Mahapatro, A. K.; Jeong, K. J.; Lee, G. U.; Janes, D. B. Sequence specific electronic conduction through polyion-stabilized double-stranded DNA in nanoscale break junctions. *Nanotechnology* **2007**, *18*, 195202.
(43) Mohammad, H.; Demir, B.; Akin, C.; Luan, B.; Hihath, J.; Oren, E. E.; Anantram, M. P. Role of Intercalation on Electrical Properties of Nucleic Acids for use in Molecular Electronics. *Nanoscale Horizons* **2021**, *6*, 651–660.
(44) Xiang, L.; Palma, J. L.; Li, Y.; Mujica, V.; Ratner, M. A.; Tao, N. Gate-controlled conductance switching in DNA. *Nat. Commun.* **2017**, *8*, 14471.
(45) Xu, B.; Zhang, P.; Li, X.; Tao, N. Direct conductance measurement of single DNA molecules in aqueous solution. *Nano Lett.* **2004**, *4*, 1105–1108.
(46) Cuniberti, G.; Craco, L.; Porath, D.; Dekker, C. Backbone-induced semiconducting behavior in short DNA wires. *Phys. Rev. B: Condens. Matter Mater. Phys.* **2002**, *65*, 241314.
(47) Wang, H.; Cheatham, T. E.; Gannett, P. M.; Lewis, J. P. Differential electronic states observed during A–B DNA duplex conformational transitions. *Soft Matter* **2009**, *5*, 685–690.
(48) Taniguchi, M.; Kawai, T. Electronic structures of A-and B-type DNA crystals. *Phys. Rev. E* **2004**, *70*, 011913.
(49) Capobianco, A.; Caruso, T.; D'Ursi, A. M.; Fusco, S.; Masi, A.; Scrima, M.; Chatgilialoglu, C.; Peluso, A. Delocalized hole domains in Guanine-rich DNA oligonucleotides. *J. Phys. Chem. B* **2015**, *119*, 5462–5466.
(50) Luo, L.; Choi, S. H.; Frisbie, C. D. Probing hopping conduction in conjugated molecular wires connected to metal electrodes. *Chem. Mater.* **2011**, *23*, 631–645.
(51) Aggarwal, A.; Bag, S.; Venkatramani, R.; Jain, M.; Maiti, P. K. Multiscale modelling reveals higher charge transport efficiencies of DNA relative to RNA independent of mechanism. *Nanoscale* **2020**, *12*, 18750–18760.
(52) Ussery, D. W. DNA Structure: A-, B- and Z-DNA Helix Families. In *eLS*; American Cancer Society, 2002.

NOTE ADDED AFTER ASAP PUBLICATION

This paper was published on September 24, 2021. Due to production error, panel (e) was missing from the Figure 3 graphic. The corrected version was reposted on October 8, 2021.

https://doi.org/10.1021/acsanm.1c01087
ACS Appl. Nano Mater. 2021, 4, 10029–10037